Publ. Astron. Soc. Japan (2022) 00 (0), 1–12
https://doi.org/10.1093/pasj/psac059
Advance Access Publication Date: 2022 0

Discovery of a new supergiant fast X-ray transient MAXI J0709−159 associated with the Be star LY Canis Majoris

Mutsumi Sugizaki [1,*] Tatehiro Mihara [2] Kohei Kobayashi [3] Hitoshi Negoro [3] Megumi Shidatsu [4] Sean N. Pike [5] Wataru Iwakiri [6] Sota Urabe [6] Motoko Serino [7] Nobuyuki Kawai [8] Motoki Nakajima [9] Jamie A. Kennea [10] and Zhu Liu [11]

[1]National Astronomical Observatories, Chinese Academy of Sciences, 20A Datun Rd, Beijing 100012, China
[2]RIKEN, 2-1 Hirosawa, Wako, Saitama 351-0198, Japan
[3]Department of Physics, Nihon University, 1-8 Kanda Surugadai, Chiyoda-ku, Tokyo 101-8308, Japan
[4]Department of Physics, Ehime University, 2-5 Bunkyocho, Matsuyama, Ehime 790-8577, Japan
[5]Cahill Center for Astronomy and Astrophysics, California Institute of Technology, Pasadena, CA 91125, USA
[6]Department of Physics, Chuo University, 1-13-27 Kasuga, Bunkyo-ku, Tokyo 112-8551, Japan
[7]Department of Physical Sciences, Aoyama Gakuin University, 5-10-1 Fuchinobe, Chuo-ku, Sagamihara, Kanagawa 252-5258, Japan
[8]Department of Physics, Tokyo Institute of Technology, 2-12-1 Ookayama, Meguro-ku, Tokyo 152-8551, Japan
[9]School of Dentistry at Matsudo, Nihon University, 2-870-1 Sakaecho-nishi, Matsudo, Chiba 101-8308, Japan
[10]Department of Astronomy and Astrophysics, Pennsylvania State University, 525 Davey Laboratory, University Park, PA 16802, USA
[11]Max Planck Institute for Extraterrestrial Physics, Giessenbachstrasse 1, D-85748 Garching, Germany

*E-mail: mutsumi@nao.cas.cn

Received 2022 June 14; Accepted 2022 July 5

Abstract

We report on the discovery of a new supergiant fast X-ray transient (SFXT), MAXI J0709−159, and its identification with LY CMa (also known as HD 54786). On 2022 January 25, a new flaring X-ray object, named MAXI J0709−159, was detected by the Monitor of All-sky X-ray Image (MAXI). Two flaring activities were observed in two scans ∼3 hr apart, where the 2–10 keV flux reached 5×10^{-9} erg cm^{-2} s^{-1}. During the period, the source exhibited a large spectral change, suggesting that the absorption column density $N_{\rm H}$ increased from 10^{22} to 10^{23} cm^{-2}. A NuSTAR follow-up observation on January 29 identified a new X-ray source with a flux of 6×10^{-13} erg cm^{-2} s^{-1} at a position consistent with LY CMa, which has been identified as a B supergiant as well as a Be star, located at a 3 kpc distance. The observed X-ray activity, characterized by short ($\lesssim$several hours) duration, rapid ($\lesssim$ a few seconds) variabilities accompanied by spectral changes, and a large luminosity swing (10^{32}–10^{37} erg s^{-1}), agree with those of SFXTs. On the other

hand, optical spectroscopic observations of LY CMa reveal a broad Hα emission line, which may indicate the existence of a Be circumstellar disk. These results suggest that the optical companion, LY CMa, certainly has a complex circumstellar medium including dense clumps.

Key words: stars: Be — stars: invdividual (LY Canis Majoris, HD 54786) — stars: neutron — supergiant — X-rays: binaries

1 Introduction

MAXI (the Monitor of All-sky X-ray Image: Matsuoka et al. 2009) on the International Space Station (ISS) has been continuously scanning almost the entire sky every ISS orbital cycle (∼92 min) since its in-orbit operation started in 2009. It provides us with a unique opportunity to discover new objects and study their transient behaviors. In fact, we have discovered 31 new X-ray objects including 14 black hole binaries, 13 neutron star binaries, and one white dwarf binary, that appeared in our Galaxy and the Small Magellanic Cloud (e.g., Mihara et al. 2022). The data also enable us to study their variabilities on time scales from hours to over 12 yr. To uncover the nature of these new transient objects, prompt follow-up observations with large-area X-ray telescopes as well as multi-wavelength observations from both space and ground observatories are essential. The MAXI nova-alert system (Negoro et al. 2016) and prompt coordinated observations with the Swift, NICER, and NuSTAR satellites have been working effectively for these transient studies, such as the ignition of a classical nova, MAXI J0158−744 (Morii et al. 2013); a new Be X-ray binary pulsar, MAXI J0903−531 (Tsygankov et al. 2021); and a faint and short-duration black hole binary candidate, MAXI J1848−015 (Pike et al. 2022).

On 2022 January 25, MAXI discovered a new X-ray transient with an instantaneous 4–10 keV flux of 270 mCrab (∼5×10^{-9} erg cm^{-2} s^{-1}), named MAXI J0709−159 (hereafter MAXI J0709), in the constellation Canis Majoris (Serino et al. 2022). The source was first detected during the scan transit at UT 10:42, but not detected in the next scan transit at UT 12:15. However, it was detected again in the subsequent scan at UT 13:48 (Kobayashi et al. 2022). This means that the source exhibited a large intensity variation within three hours. Three hours after the MAXI discovery, NICER (the Neutron star Interior Composition ExploreR; Gendreau et al. 2012) started multiple pointing observations covering almost the entire region of the MAXI position error (circle of radius ∼0.°2). The new transient was successfully detected with the pointing observation carried out 6 min after the MAXI scan at UT 13:46. The NICER observations refined the source position with an error of 3′ and also revealed that the X-ray flux had declined by a factor of ∼10 from the MAXI observations (Iwakiri et al. 2022).

From 2022 January 19–February 18, the Swift X-ray satellite (Gehrels et al. 2004) stopped normal operation because of trouble with the attitude control system.[1] Hence, we applied for a NuSTAR (Nuclear Spectroscopic Telescope Array; Harrison et al. 2013) ToO (time of opportunity) observation. The NuSTAR observation was carried out on 2022 January 29, four days after the discovery. The result revealed a new point source within the error circle of the MAXI J0709 position uncertainty. The position of the new source is consistent with LY CMa (also known as HD 54786), which has been identified as a Be star (Negoro et al. 2022; Nesci 2022). In Gaia Early Data Release 3, the distance is estimated to be $D = 3.03^{+0.31}_{-0.27}$ kpc (Bailer-Jones et al. 2021).[2] From optical follow-up observations and archival data analysis, Bhattacharyya et al. (2022) suggested that LY CMa could be an evolved Be star, rather than a main sequence star or a supergiant. A radio observation was carried out on 2022 January 31 with the MeerKAT radio telescope, but no significant emission was detected at 1.28 GHz and the 3σ upper limit was estimated to be 57 μJy (Rhodes et al. 2022) Finally, the Swift ToO observation was carried out on 2022 February 23.

In this paper, we report the discovery of the new transient MAXI J0709 and the results of the MAXI, NuSTAR, Swift, and eROSITA observations of the identified X-ray object. We also report an optical follow-up observation of the optical counterpart at Chuo University. Based on the obtained results, we discuss the nature of the new X-ray object. Throughout the paper, errors represent 90% confidence limits of statistical uncertainties unless otherwise specified.

2 MAXI observations and data analysis

The MAXI gas slit camera (GSC; Mihara et al. 2011; Sugizaki et al. 2011) consists of 12 identical camera units,

[1] ⟨https://swift.gsfc.nasa.gov/news/2022/safe_mode.html⟩.

[2] ⟨https://vizier.u-strasbg.fr/viz-bin/VizieR-3?-source=I/352⟩.

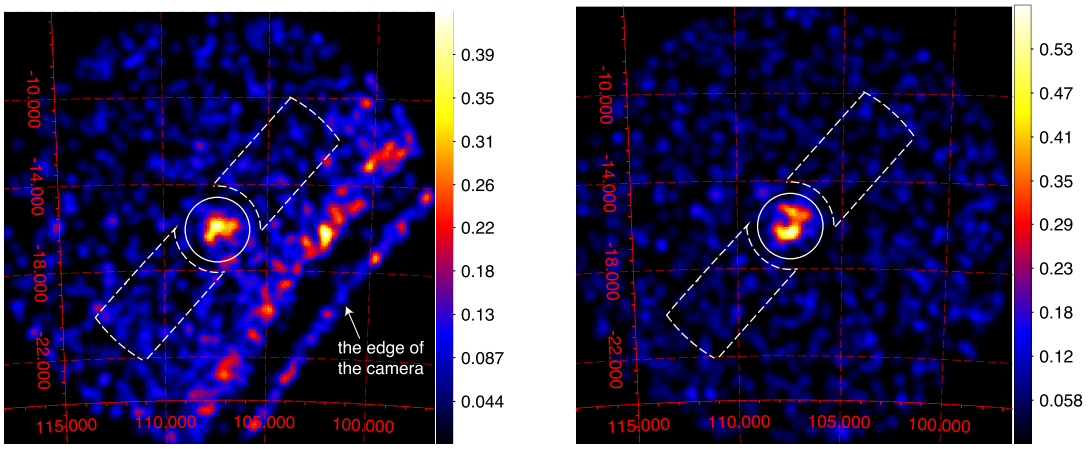

Fig. 1. GSC 2–20 keV images obtained by GSC_4 (left) and GSC_5 (right) units, within 10° of MAXI J0709 at Scan-A (UT 10:39–10:46 on January 25). The image is smoothed with a Gaussian kernel of $\sigma = 2°$. The source and background regions used in the spectral analysis are shown by the solid and dashed lines, respectively.

namely GSC_0, . . . , GSC_9, GSC_A, GSC_B. Utilizing the two wide (160° × 3°) FOVs, GSC scans the whole sky every 92 min. We investigated the X-ray activities of the new transient MAXI J0709 on time scales shorter than each scan transit (∼40 s) and longer than the scan cycle (∼92 min) using the GSC data. We here employ GSC event files of the process version 2.1, taken via the low-speed telemetry interface, and perform a data analysis using the MAXI software included in HEASoft version 6.29 and the calibration database (CALDB) version 20210504 released from the JAXA data archive.[3]

2.1 GSC light curve

We extracted GSC light curves of MAXI J0709 by fitting each GSC scan image with a model consisting of a point-spread function (PSF) for the target source and a uniform background (Morii et al. 2016). The source position was fixed at the position parameters refined by the NuSTAR observation (subsection 3.1). Figure 1 shows GSC 2–20 keV images taken by the GSC_4 and GSC_5 units, when MAXI J0709 was first detected on 2022 January 25 (MJD 59604). Within 10 days before and after the first detection, the source had been observed by either or both of these two GSC units.

Figure 2 shows the obtained 2–4 and 4–10 keV light curves from two days before to five days after the first detection. The data gap from MJD 59603.2 to 59604.3 corresponds to the period when the source position was shadowed by the frame structure in the GSC detector.[4] After the data gap, there was no significant flux in the

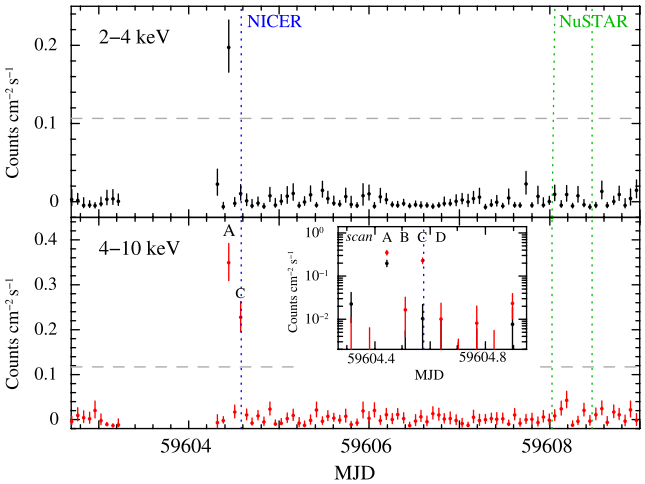

Fig. 2. GSC light curves of MAXI J0709 in the 2–4 keV (black) and 4–10 keV (red) bands. Horizontal dashed lines represent the expected count rates for a 100 mCrab source, 0.106 counts cm^{-2} s^{-1} at 2–4 keV and 0.117 counts cm^{-2} s^{-1} at 4–10 keV. Vertical dotted lines represent the epoch of the NICER observation start (blue) and the NuSTAR observation period (green). The inset is a log-linear plot of the 0.7 d around the source onset, where Scan-A, B, C, D are annotated.

two scans. Then, the first X-ray activity was detected in the scan transit at UT 10:42 (MJD 59604.446, Scan-A). The source count rates averaged over the scan transit were $0.19^{+0.03}_{-0.03}$ counts cm^{-2} s^{-1} (180 mCrab) at 2–4 keV and $0.35^{+0.04}_{-0.04}$ counts cm^{-2} s^{-1} (300 mCrab) at 4–10 keV. In the next scan transit at UT 12:15 (MJD 59604.510, Scan-B), there was no significant flux over the background with 1σ upper limits of 0.005 counts cm^{-2} s^{-1} (5 mCrab) at 2–4 keV and 0.032 counts cm^{-2} s^{-1} (27 mCrab) at 4–10 keV. In the subsequent scan transit at UT 13:48 (MJD 59604.575, Scan-C), the source was detected again but only in the 4–10 keV band with $0.23^{+0.03}_{-0.03}$ counts cm^{-2} s^{-1} (200 mCrab). This means that the source intensity changed every scan

[3] ⟨https://www.darts.isas.jaxa.jp/astro/maxi/data.html⟩.

[4] See also the light curve on the MAXI homepage ⟨http://maxi.riken.jp/pubdata/v7lrkn/J0709-161/⟩.

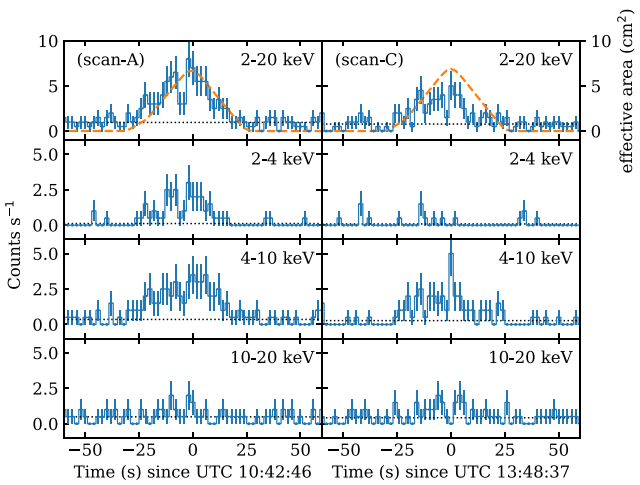

Fig. 3. GSC count rates during the scan transits centered at UT 10:42 (Scan-A) and 13:48 (Scan-C) on 2022 January 25. Data are binned every 2 s. Dotted lines represent the background levels. Dashed lines in the top panels show the effective-area variation for the MAXI J0709 sky position.

transit by a factor of $\gtrsim$10 and also the spectrum changed. In the following scans after MJD 59604.639 (Scan-D), the source activity went down below the GSC sensitivity limit.

We then investigated the source variability within each scan transit of Scan-A and Scan-C, which include significant source photons. Figure 3 shows count rate variations during Scan-A and Scan-C, compared with the effective-area variations for the source position and the backgrounds estimated from the data in the adjacent source-free region. In Scan-A, the 2–20 keV count rate roughly traces the effective-area variation, indicating that the photon flux was approximately constant during the scan transit. However, at the middle of the transit, a dip-like structure lasting for ~4 s is clearly seen. We fitted the data around the dip with a constant-flux model, i.e., a normalized effective-area curve plus background. The result gives a Cash statistic (C-stat; Cash 1979) of 7.5 for three degrees of freedom (d.o.f.), meaning that the constant model is rejected with a confidence of >90%. In Scan-C, the 4–10 keV count rate shows a sharp peak at the center of the scan. We performed model fitting in the same way as in Scan-A and obtained a similar result, with the constant-flux model being rejected with a confidence of >95%. These results suggest the source has a rapid time variability on time scales of a few seconds or less.

We also investigated the past source activity from the beginning of the MAXI in-orbit operation in 2009 August. At a distance of 0.°55 from the refined MAXI J0709 position, another X-ray source, 3MAXI J0708−155, was reported in the seven-year MAXI/GSC source catalog (Hori et al. 2018). There, the object is identified as a blazar, PKS 0706−15. Although this nearby X-ray object can be distinguished from MAXI J0709 with the MAXI/GSC position accuracy ($\lesssim$0.°2), the PSFs of these two objects have an overlap, which causes source confusion. We carefully estimate the amount of the possible confusion and confirmed that MAXI J0709 had not shown any significant (>4σ) flaring activity until the present event.

2.2 X-ray spectra of two flaring events

Next, we analyzed the GSC energy spectra in Scan-A and Scan-C in detail. Source spectra were extracted from a circular region within 1.°5 from the source position. To avoid the high background area near the edge of the detector in GSC_4 (figure 1), background spectra were extracted from the overlap region between an annulus of inner and outer radii of 2° and 7°, and a 14° × 3° rectangle along the scan direction, both centered at the source position. These source and background regions are illustrated in figure 1. We confirmed that background-subtracted spectra were consistent between GSC_4 and GSC_5, and then added them together to give GSC_4 + GSC_5 spectra.

Figure 4 shows the obtained source-region spectra in Scan-A and Scan-C. As expected from the light curves in figure 2, the Scan-C spectrum has a lower-energy cutoff below 4 keV. We performed model fitting on XSPEC version 12.11.1 (Arnaud 1996) employing the C-statistic method. The energy response matrix for each data was calculated with `mxgrmfgen` included in HEASoft. Also, spectral data were binned so that each bin contains at least one event. We first checked that background spectra were well represented by a two-power-law model. Then, we fitted source-region spectra including backgrounds and background spectra simultaneously to determine the source spectral model.

First, we fitted each of the Scan-A and Scan-C spectra with a power law with an interstellar-medium (ISM) absorption. We hereafter employed the Tuebingen–Boulder ISM absorption model (`TBabs`) with the solar abundances provided by Wilms, Allen, and McCray (2000). Both fits to the Scan-A and Scan-C spectra were acceptable. Table 1 summarizes the best-fitting model parameters. While the power-law photon indices, $\Gamma = 2.3^{+0.7}_{-0.6}$ in Scan-A and $2.7^{+1.2}_{-1.0}$ in Scan-C, are consistent within the errors, the absorption column densities, $N_{\rm H} = 5.5^{+5.8}_{-4.8} \times 10^{22}$ cm^{-2} in Scan-A and $58^{+53}_{-30} \times 10^{22}$ cm^{-2} in Scan-C, are significantly different. The $N_{\rm H}$ value in Scan-A is larger than the Galactic H I density, 0.5×10^{22} cm^{-2}, in the source direction (HI4PI Collaboration 2016). We then fitted the two spectra with a common Γ simultaneously. The fit was accepted similarly, and the best-fitting $\Gamma = 2.4^{+0.6}_{-0.5}$ was obtained. In this case,

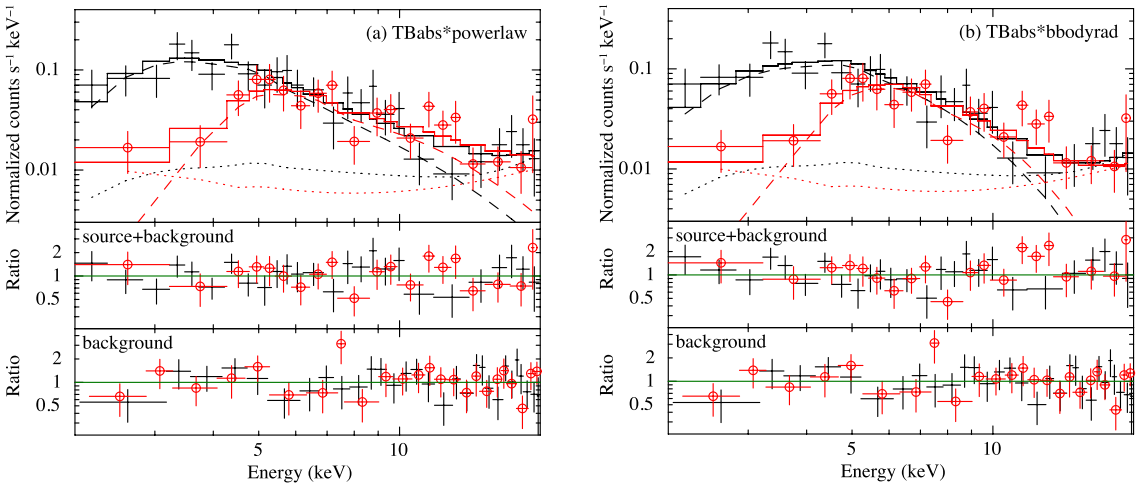

Fig. 4. GSC energy spectra fitted with (a) power law and (b) blackbody with an interstellar absorption. In all panels, black dots and red circle marks represent Scan-A and Scan-C data, respectively. (Top) Observed source-region spectra, folded with the GSC response function. Dashed lines, dotted lines, and solid histograms represent model spectra for source, background, and source+background, respectively. (Middle) Data-to-model ratio of source-region (including background) spectra. (Bottom) Data-to-model ratio of background spectra. For visual clarity, plotted data are rebinned.

Table 1. Best-fitting spectral parameters of MAXI J0709.

Parameter	Scan-A		Scan-C
	— Model: TBabs*powerlaw —		
$N_{\rm H}$ (10^{22} cm^{-2})	$5.5^{+5.8}_{-4.8}$		58^{+53}_{-30}
Γ	$2.3^{+0.7}_{-0.6}$		$2.7^{+1.2}_{-1.0}$
$F_{\rm abs}$*	$0.48^{+0.08}_{-0.07}$		$0.29^{+0.07}_{-0.06}$
$F_{\rm unabs}$†	$0.7^{+0.4}_{-0.2}$		$1.8^{+3.6}_{-1.1}$
C-stat/d.o.f.	202/267		177/210
$N_{\rm H}$ (10^{22} cm^{-2})	$6.2^{+5.3}_{-4.4}$		51^{+27}_{-20}
Γ		$2.4^{+0.6}_{-0.5}$	
$F_{\rm abs}$*	$0.48^{+0.08}_{-0.07}$		$0.29^{+0.06}_{-0.06}$
$F_{\rm unabs}$†	$0.7^{+0.3}_{-0.2}$		$1.4^{+1.4}_{-0.6}$
C-stat/d.o.f.		379/478	
	—Model: TBabs*bbodyrad —		
$N_{\rm H}$ (10^{22} cm^{-2})	<2.2		27^{+32}_{-21}
$T_{\rm BB}$ (keV)	$1.5^{+0.2}_{-0.2}$		$2.2^{+0.8}_{-0.5}$
$R_{\rm BB}$‡ (km)	$3.1^{+0.9}_{-0.7}$		$1.8^{+1.5}_{-0.9}$
$F_{\rm abs}$*	$0.50^{+0.09}_{-0.08}$		$0.31^{+0.07}_{-0.06}$
$F_{\rm unabs}$†	$0.50^{+0.09}_{-0.08}$		$0.6^{+0.5}_{-0.2}$
C-stat/d.o.f.	202/267		179/210
$N_{\rm H}$ (10^{22} cm^{-2})	<1.5		48^{+32}_{-22}
$T_{\rm BB}$ (keV)		$1.6^{+0.2}_{-0.2}$	
$R_{\rm BB}$‡ (km)	$2.8^{+0.7}_{-0.6}$		$3.7^{+2.1}_{-1.2}$
$F_{\rm abs}$*	$0.51^{+0.08}_{-0.08}$		$0.32^{+0.07}_{-0.06}$
$F_{\rm unabs}$†	$0.51^{+0.08}_{-0.08}$		$0.9^{+0.7}_{-0.4}$
C-stat/d.o.f.		385/478	

*Absorbed 2–10 keV flux in 10^{-8} erg cm^{-2} s^{-1}.
†Unabsorbed 2–10 keV flux in 10^{-8} erg cm^{-2} s^{-1}.
‡Blackbody radius in km. Distance of 3 kpc assumed.

the absorption-corrected 2–10 keV fluxes are consistent between Scan-A and Scan-C at $\sim 0.5 \times 10^{-8}$ erg cm^{-2} s^{-1}.

We also fitted the two spectra with a blackbody model (`bbodyrad`) with an interstellar absorption. The fits were acceptable in both Scan-A and Scan-C, like the fits with a power-law model. The obtained model parameters are summarized in table 1. There, the blackbody model normalizations are given by a source radius $R_{\rm BB}$. $N_{\rm H}$ of Scan-A was constrained only by the upper limit ($<2.2 \times 10^{22}$ cm^{-2}). Although the blackbody temperatures, $T_{\rm BB} = 1.5^{+0.2}_{-0.2}$ keV in Scan-A and $2.2^{+0.8}_{-0.5}$ keV in Scan-C, were slightly different, we tried a simultaneous fit to the two spectra with a common $T_{\rm BB}$. The fit was still acceptable and the best-fitting $T_{\rm BB} = 1.6^{+0.2}_{-0.2}$ keV was obtained.

3 NuSTAR observation and data analysis

The NuSTAR observation of MAXI J0709 was carried out in 2022 January 29 UT 00:21–11:21 (OBSID: 90801304002), with a net exposure of 18 ks. We performed data analysis using the NuSTAR Data Analysis Software `nustardas` version 2.1.1 included in HEASoft version 6.29 and the CALDB version 20220215, following the NuSTAR Data Analysis Quick Start Guide[5] and the NuSTAR Data Analysis Software Guide.[6] The unfiltered event files were first reprocessed by `nupipeline`. According to the recommendations given by the NuSTAR team, we screened high-background-rate data taken during the South

[5] ⟨https://heasarc.gsfc.nasa.gov/docs/nustar/analysis/nustar_quickstart_guide.pdf⟩.
[6] ⟨https://heasarc.gsfc.nasa.gov/docs/nustar/analysis/nustar_swguide.pdf⟩.

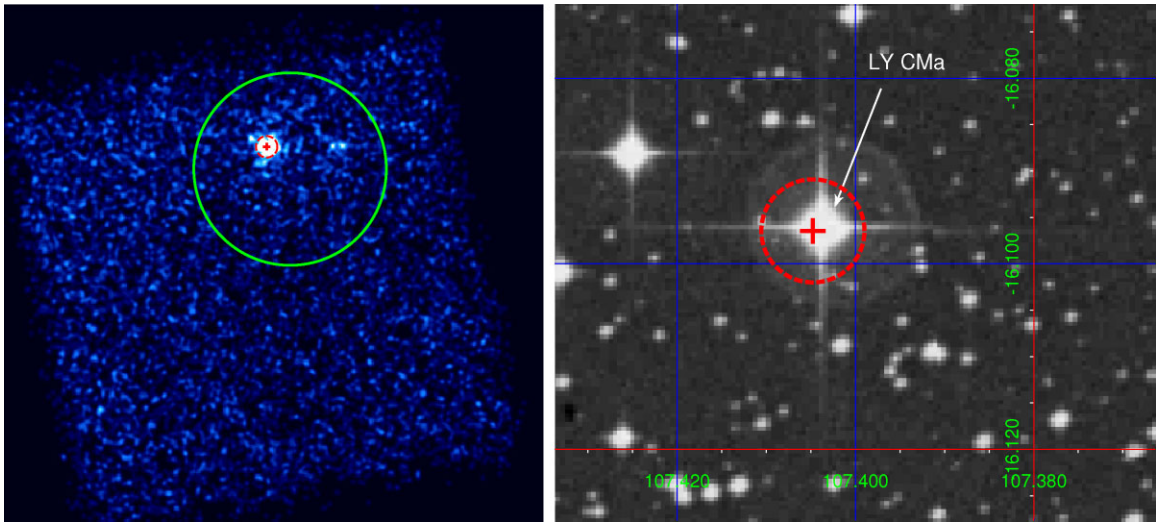

Fig. 5. (Left) NuSTAR/FPMA+FPMB 3–20 keV image around the source, where Gaussian smoothing is applied to the image with a radius of 2 pixels. The red cross and dashed circle indicate the best-fitting position and the error (20″, including the systematic error) determined with NuSTAR, respectively. The NICER error circle (with a 3′ radius) is also shown by the green line. (Right) Optical image of the DSS (original Digitized Sky Survey). The NuSTAR source position and error are shown by the red cross and dashed circle.

Atlantic Anomaly (SAA) passages by combining options SAAMODE = optimized and TENTACLE = yes with the default SAA calculation option (saacalc = 3). The resultant cleaned event files were used to obtain the image, light curve, and time-averaged spectrum.

3.1 Localization and optical identification with the NuSTAR image

We produced the NuSTAR images from the cleaned event files using `nuproducts`. In figure 5 (left panel), we show the NuSTAR 3–20 keV image. A significant point source was solely detected within the error circle (radius = 3′) of the MAXI J0709 position determined by the NICER observation (Iwakiri et al. 2022). To determine the accurate source position, we performed image fitting using `sherpa` included in the Chandra Interactive Analysis of Observation (ciao; version 4.14). To improve the photon statistics, images of FPMA and FPMB are combined and binned by 2 × 2 pixels. The obtained image in the 4′ × 4′ region around the count peak was then fitted with a model consisting of a 2D Gaussian function for the target point source and a flat surface for the background. There, we employed the Cash statistics. Because the ellipticity of the 2D Gaussian was not significantly detected, the ellipticity parameter was fixed at 0 (circular). The best-fitting model parameters are the source position (α, δ) (J2000.0) = ($7^{\rm h}09^{\rm m}37\overset{\rm s}{.}1$, $-16^\circ05'47''$) with errors of 2″, and a full width at half-maximum (FWHM) of 16″ ± 2″, where errors include only statistic uncertainties. The systematic error of the NuSTAR position accuracy is estimated at ≃20″, which slightly depends on the source brightness (Lansbury et al. 2017).

Comparing the obtained NuSTAR image with the DSS (original Digitized Sky Survey) optical image provided via the Skyview website[7] in the same region (the right panel of figure 5), we identified a possible optical counterpart, LY CMa (also known as HD 54786), which is identified as a Be star (Chojnowski et al. 2015) with a spectral type of B1.5 I(b), i.e., a B supergiant (Houk & Smith-Moore 1988). From Gaia Early Data Release 3, its celestial position (α, δ) (J2000.0) = ($7^{\rm h}09^{\rm m}36\overset{\rm s}{.}9791095248$, $-16^\circ05'46\overset{''}{.}801897476$) and distance $D = 3.03^{+0.31}_{-0.27}$ kpc are well determined (Gaia Collaboration 2016, 2021; Bailer-Jones et al. 2021). The position is only 1″.8 from the NuSTAR best-fitting parameters. The direction and distance suggest that the object is located on the Perseus Arm, a major spiral arm of our Galaxy.

3.2 Light curves

We produced NuSTAR light curves in three energy bands, 3–20, 3–5, and 5–20 keV, with `nuproducts`. Source data were extracted from a circular region with a radius of 30″ centered at the LY CMa position, and background data were extracted from another circle with a radius of 60″ in a source-free region. In this step, a barycentric time correction was applied to event files, assuming the source position of LY CMa. The data of FPMA and FPMB were combined with the ftool `lcmath`. In figure 6 we plot the obtained

[7] ⟨http://skyview.gsfc.nasa.gov⟩.

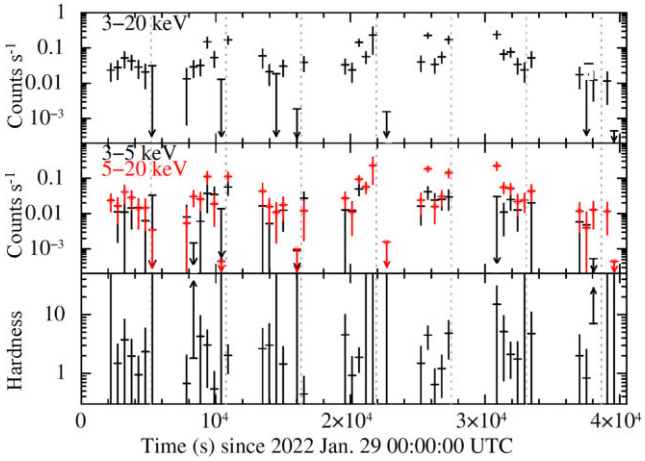

Fig. 6. NuSTAR background-subtracted light curves in 3–20 (top), 3–5 (middle; black crosses), and 5–20 keV (middle; red open squares) in 512 s bins, and the hardness ratio between the latter two bands (bottom). The background level is 0.01–0.02 counts s^{-1} at 3–20 keV during the observation. Vertical dashed lines represent the epochs of MAXI scans in figure 2.

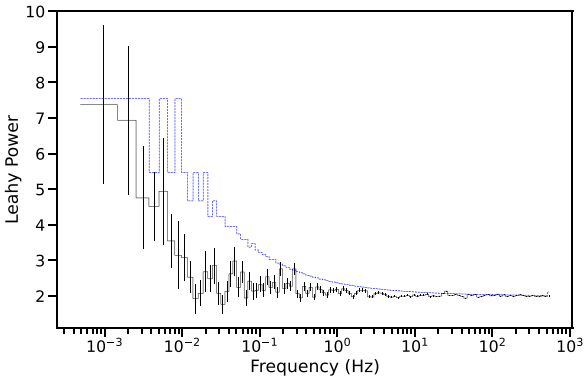

Fig. 7. Power spectrum calculated using 3-20 keV NuSTAR FPMA and FPMB data, averaged over the entire observation period. The blue dashed line represents the 3σ detection level of periodicity.

light curves in the the energy bands and the 5–20 to 3–5 keV hardness ratio in 512 s bins. The 3–20 keV light curve shows flux variation by factor of $\lesssim$3 on time scales of $\gtrsim 10^2$ s. The middle panel suggests that the variation is larger in the higher band (i.e., the source becomes harder with increasing flux), although this is not clear in the hardness-ratio variation.

3.3 Pulsation search

In order to search for coherent pulsations, we produced a power density spectrum (PDS) from the FPMA+FPMB data, which is shown in figure 7. We first barycenter corrected the time of arrival for each photon using the source position as determined using the automatic centroiding function in DS9 (Joye & Mandel 2003). We used JPL ephemeris DE-430 and NuSTAR clockfile v138. We extracted events with energy 3–20 keV using a source

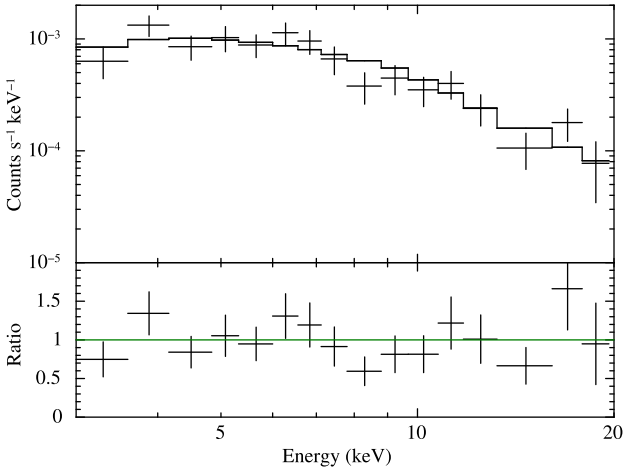

Fig. 8. (Top) Time-averaged NuSTAR/FPMA+FPMB background-subtracted, response-folded spectrum. The solid line represents the best-fitting absorbed power-law model. (Bottom) Data-to-model ratio. The data in this figure have been rebinned for visual clarity.

region with radius 30″. Next we used the Python package Stingray (Huppenkothen et al. 2019) to produce the frequency amplitude difference-corrected PDS (Bachetti & Huppenkothen 2018), which corrects for timing effects due to deadtime. We specified a time resolution of 2^{-10} s and a light-curve segment size of 1024 s, resulting in 13 individual PDS, which we averaged to produce the PDS shown. The PDS has been rebinned logarithmically for clarity. We also calculated the 3σ detection level per logarithmic frequency bin using the formalism described in Leahy et al. (1983), which we show as a blue dashed line.

We did not detect any significant periodicity, but we note that our timing analysis is severely limited due to a small number of photons (<300 total). As such we cannot rule out the presence of pulsations or other timing signatures.

3.4 Time-averaged spectrum

Figure 8 shows the time-averaged NuSTAR spectrum, which was extracted with `nuproducts` using the same source and background regions as in the light-curve analysis (subsection 3.2). The FPMA and FPMB spectra were combined with the ftool `addspec` to improve statistics, and binned so that each bin contains at least one count. We confirmed that the results did not change even if the data of FPMA and FPMB were analyzed separately.

We fitted the obtained spectrum with an absorbed power-law model (`TBabs*powerlaw`) on XSPEC employing the W statistic. The results showed the fit statistic $W = 148$ for 184 d.o.f. and the best-fitting $\Gamma = 1.7^{+0.5}_{-0.2}$. $N_{\rm H}$ was constrained only by the upper limit, $<1.1 \times 10^{23}$ cm^{-2}, which is consistent with the result of the MAXI/GSC Scan-A spectrum (table 1 in subsection 2.2). From the best-fitting model, the absorbed and absorption-corrected 2–10 keV

fluxes were estimated to be $6 \pm 1 \times 10^{-13}$ and $6^{+3}_{-1} \times 10^{-13}$ erg cm^{-2} s^{-1}, respectively. These spectral parameters are consistent with those given by Bhattacharyya et al. (2022), which utilized the same NuSTAR data.

Although there is no emission-line feature in the NuSTAR spectrum, we tested the possibility of a narrow iron-Kα emission line. We added a Gaussian function with a fixed centroid of 6.4 keV and a fixed width of 0 eV to the power-law model, and then fitted it to the data. As a result, the 90% upper limit on the iron-Kα line flux was estimated to be 4×10^{-6} photons cm^{-2} s^{-1}, which corresponds to an equivalent width (EW) of 0.6 keV.

4 Swift observation and upper limit

A ToO observation by the Neil Gehrels Swift Observatory (Gehrels et al. 2004) was carried out on 2022 February 23 (MJD 59634.62), 30 days after the discovery, with a total exposure time of 989 s. No X-ray source was detected with a 3σ upper limit of 0.008 XRT counts s^{-1} at the position of LM CMa. Assuming the spectral parameters given in table 1, this provides an upper limit on the flux of 2×10^{-12} erg cm^{-2} s^{-1} (0.3–10 keV) for the Scan-A parameters, and 1.3×10^{-12} erg cm^{-2} s^{-1} (0.3–10 keV) for the Scan-C parameters, where the flux is not corrected for absorption. These upper limits are consistent with the detected flux by NuSTAR.

5 eROSITA upper limits on the past activity

The Spectrum-Roentgen-Gamma (Spektr-RG, SRG) X-ray observatory (Sunyaev et al. 2021) has been performing an all-sky survey since 2019 December. The satellite carries two kinds of X-ray telescopes, the extended ROentogen Survey with an Imaging Telescope Array (eROSITA; Predehl et al. 2021), and the Mikhail Pavllinsky Astronomical Roentgen Telescope (ART-XC; Pavlinsky et al. 2021), which cover the 0.2–8 and 4–30 keV energy bands, respectively. The eROSITA all-sky survey (eRASS) has been carried out by consecutive scans of the entire sky, each of which is completed in six months. It currently achieves the best sensitivity among all-sky X-ray surveys that have ever been performed.

The sky position of MAXI J0709 was covered by eROSITA in the past four eRASSs as listed in table 2. All of the eROSITA data are calibrated and cleaned using the pipeline version 946 of the eROSITA Science Analysis Software System (eSASS, Brunner et al. 2022). No significant X-ray emission at the position of LY CMa was detected in either individual eRASSs or the combined dataset. We estimated a 3σ upper limit of 4×10^{-13} erg cm^{-2} s^{-1} in the 2–10 keV band using all the eRASS data and assuming a typical power-law spectrum of $\Gamma = 2$ and interstellar absorption corresponding to the Galactic H I density $N_{\rm H} = 0.5 \times 10^{22}$ cm^{-2}.

Table 2. eRASS observations on the MAXI J0709 position (upper limits).

#*	Start time	End time	$T_{\rm exp}$†
1	2020-04-17 09:34:14	2020-04-18 01:34:44	173
2	2020-10-20 08:25:17	2020-10-21 00:25:41	156
3	2021-04-18 02:34:27	2021-04-19 06:34:33	234
4	2021-10-20 13:25:24	2021-10-21 13:25:39	219

*eRASS survey number.
†Exposure time (s).

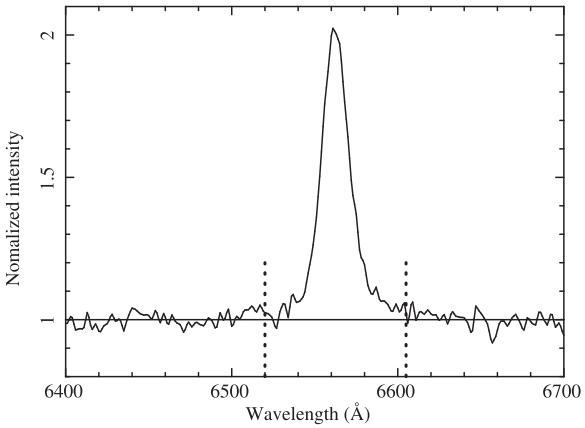

Fig. 9. Optical spectrum of LY CMa obtained by SCAT around the Hα emission line. The intensity scale is normalized by the linear continuum model. The region between the two dashed lines represents the range of the Hα line employed in the EW estimate.

6 Optical spectroscopy with SCAT

The Spectroscopic Chuo university Astronomical Telescope (SCAT) is a 355-mm diameter optical telescope equipped with an ATIK 460EX CCD camera and a Shelyak Alpy 600 spectrometer, located at the Chuo Univeristy Korakuen campus, Tokyo, Japan (Kawai et al. 2022). The spectral resolution is $R \sim 600$.

The SCAT observation of LY CMa was carried out on 2022 January 28 from UT 11:32 to 14:48 (approximately three days after the MAXI trigger) with a net exposure of 8610 s. The result clearly showed a strong Hα emission line. The FWHM of the Hα line was 19 Å, which is significantly larger than that of the Ne line in the calibration lamp (FWHM = 10 Å). Next, we estimated the line EW. To determine the continuum level, we fitted the observed spectrum excluding the Hα-line range with a linear function. Figure 9 shows the line profile normalized by the best-fitting continuum model, where the Hα-line range was assumed to

be from 6520 to 6605 Å. By integrating the profile, the EW was estimated to be −23 Å. This is consistent with the result of the Foligno Observatory low-resolution ($R \sim 50$) spectrum taken on the same day (Nesci 2022). We repeated the EW calculation by shifting the assumed Hα-line range, and found that the obtained EW value has an uncertainty of ∼15%.

7 Discussion

7.1 Summary of MAXI J0709−159 activities with past and follow-up observations

We here summarize the long-term activities of MAXI J0709 identified by the past and follow-up observations in the present analysis. Based on the results, we consider the nature of the new X-ray object in the next section.

The new transient MAXI J0709 was first discovered by the MAXI GSC all-sky survey on 2022 January 25. As seen in figure 2, significant X-rays were detected only in the two GSC scans, Scan-A (UT 10:42) and Scan-C (UT 14:48). In both scans, it showed flare-like time variabilities on a time scale of a few seconds (figure 3) and the 2–10 keV flux reached 5×10^{-9} erg cm^{-2} s^{-1}. At Scan-B (UT 12:15) and after Scan-C (UT 15:21), the source was not detected with the GSC sensitivity limit of 80 mCrab (1.5×10^{-9} erg cm^{-2} s^{-1} at 2–10 keV) per scan (Negoro et al. 2016). Therefore, the intensity swings between every adjacent scan from Scan-A to Scan-D exceed a factor of ∼5.

The NICER and NuSTAR follow-up observations successfully identified the new transient with a new X-ray source, whose position is consistent with LY CMa (figure 5). When NICER observed it at 6 min after the MAXI Scan-C, the X-ray flux became about 10 mCrab (at 0.2–12 keV), which is $<10^{-1}$ of that observed in Scan-C. When NuSTAR identified the new object on January 29, four days after the MAXI detections, the X-ray flux became relatively stable at around 6×10^{-13} erg cm^{-2} s^{-1}. This means that the X-ray intensity decreased by a factor of 10^{-4} in three days.

We investigated the past source activity using archival data. Until the first MAXI detection, the source had not been recognized in the MAXI GSC data for over 12 yr. The upper limit on the average source flux is 5×10^{-12} erg cm^{-2} s^{-1} (Hori et al. 2018). The object had not been recorded in any X-ray source catalog including the ROSAT all-sky survey catalog (Boller et al. 2016). Also, eROSITA all-sky surveys, which observed the MAXI J0709 position four times from 2020 to 2021, did not find a significant X-ray source with a 3σ upper limit of 4×10^{-13} erg cm^{-2} s^{-1} (section 5), which is lower than the flux observed by NuSTAR. This suggests that the source activity at the NuSTAR observation was still higher than that before the discovery.

In figure 10, the long-term activities after the discovery of MAXI J0709 are summarized. The X-ray intensity variation clearly reveals that the activity declined at $\sim 10^4$ s ($\simeq$3 hr). In the figure, the right-hand ordinate represents the luminosity calculated from the flux at a source distance of 3 kpc. The observed flux range of 10^{-13}–10^{-8} erg cm^{-2} s^{-1} corresponds to 10^{32}–10^{37} erg s^{-1} in the luminosity.

We also carried out an optical spectroscopic observation of the optical counterpart LY CMa on January 28, three days after the discovery, and then confirmed the Hα emission line (section 6) as reported in Nesci (2022). The EW of the Hα line was estimated to be −23 Å with an uncertainty of ∼15%. Bhattacharyya et al. (2022) also performed optical follow-up observations and reported that the Hα EW was −17.6 Å on February 2 and −16.9 Å on February 3. The results suggest that the EW might change in these three days.

7.2 Classification of the new X-ray object in high-mass X-ray binaries

As discussed in the previous section and summarized in figure 10, the observed X-ray activity of MAXI J0709 is characterized by an initial flaring phase of ≈3 hr with a rapid (∼ few seconds) variability reaching the peak luminosity $\simeq 5 \times 10^{36}$ erg s^{-1}, and a subsequent decay phase lasting for at least several days with a luminosity $\sim 10^{32}$–10^{33} erg s^{-1} and a moderate variation. The rapid variability naturally leads us to the idea of X-ray binaries embedding compact objects, neutron stars or black holes, where the transient behavior can be explained by the change in the mass accretion onto the compact object. In the present MAXI J0709 case, the mass-donating stellar companion is identified with LY CMa, which has a spectral type of B1.5 I(b) (Houk & Smith-Moore 1988) and also an identification as a Be star (Chojnowski et al. 2015). Hence, we consider the detailed scenario to explain all the observed results in comparison with other high-mass X-ray binaries (HMXBs) that have been well studied.

The initial flaring behavior of the short duration ($\lesssim$ several hours) and the rapid variability (on a time scale of a few seconds) agree well with the properties of supergiant fast X-ray transients (SFXTs), a possible subclass of HMXBs that consist of OB supergiants and neutron stars showing sporadic short-duration ($\lesssim$ several hours) outbursts (Sguera et al. 2006; Bozzo et al. 2015; Sidoli & Paizis 2018; see also Kretschmar et al. 2019 for a review). The observed luminosity range from 10^{32} to 10^{37} erg s^{-1} agrees with those from their quiescent value to the flaring peak. The X-ray spectra fitted with a power law of $\Gamma \simeq 2$ in both the MAXI and NuSTAR data are also typical as SFXTs, which have power-law spectra with $\Gamma \sim 1(\pm 1)$ (Pradhan et al. 2018).

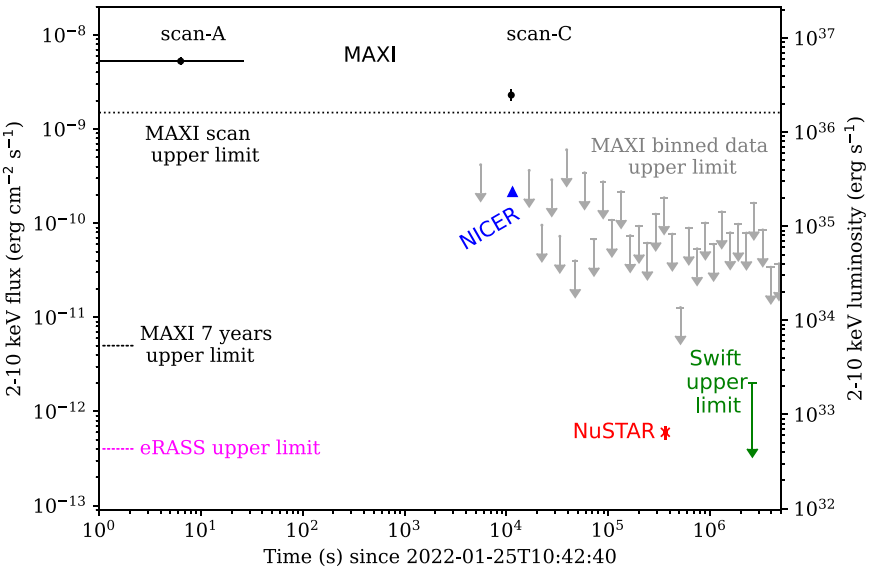

Fig. 10. MAXI J0709 long-term X-ray activity since the first MAXI detection at UT 10:42 on 2022 January 25, obtained from the present analysis of the MAXI, NuSTAR, Swift, and eROSITA data and the NICER result reported by Iwakiri et al. (2022). Upper limits from the logarithmically binned MAXI/GSC light curve are shown by gray arrows.

During the initial flaring phase, the X-ray spectrum changed dramatically so that $N_{\rm H}$ changed from 10^{22} to 10^{23} cm^{-2} in $\sim$3 hr (figure 4). $N_{\rm H} \gtrsim 10^{23}$ cm^{-2} at the MAXI GSC Scan-C is significantly higher than the Galactic H I density $\simeq 0.5\times\ 10^{22}$ cm^{-2}, and also comparable to the highest among those of SFXTs that have ever been reported (Pradhan et al. 2018). So far, a similar spectral change has been observed in IGR J18410−0535, and it was explained by a scenario that the compact object (neutron star) just plunged into a dense clump in the circumstellar medium (Bozzo et al. 2011). The present result can be considered similarly.

Also, the iron-K line was not significantly detected in either MAXI or the NuSTAR spectrum. From the NuSTAR data, the upper limit on the equivalent width $\mathrm{EW_{FeK}} < 0.6$ keV was estimated. In general, X-ray spectra of SFXTs have lower $N_{\rm H}$ and lower $\mathrm{EW_{FeK}}$ than those of classical supergiant HMXBs with persistent X-ray activities (Giménez-García et al. 2015; Pradhan et al. 2018). This implies that SFXTs have sparser and more clumpy circumstellar media than classical supergiant HMXBs. The present results support this scenario.

To explain the short duration (several hours) and the extremely large dynamic range (10^3–10^4) from quiescence to the peak in the SFXT outbursts, some mechanism to inhibit accretion such as magnetic and/or centrifugal barriers (Grebenev & Sunyaev 2007; Bozzo et al. 2008) is required. If the compact objects in SFXTs are magnetized neutron stars, the observed X-ray variations may relate to the neutron star rotation. In fact, coherent pulsations were detected in several SFXTs. We performed a period search with the NuSTAR data, but could not find a significant periodicity (subsection 3.3). The results are consistent with most major well-known SFXTs, in which periodicity has not been detected even though deep observations have been carried out (e.g., Bozzo et al. 2010; Ferrigno et al. 2020). This may indicate that the neutron stars have very long spin periods and the X-ray variations only come from the magnetic and centrifugal gating mechanism (Bozzo et al. 2008), or that the accretions are in a quasi-spherical accretion regime (Shakura et al. 2012).

7.3 Is MAXI J0709−159 an evolved Be fast X-ray transient?

So far, we have discussed the nature of MAXI J0709 based on the X-ray results that agree well with typical SFXTs. Meanwhile, the optical counterpart LY CMa is also identified as a Be star (Chojnowski et al. 2015). In fact, optical follow-up observations have confirmed the broad Hα line, which indicates a Be circumstellar disk (section 6). Bhattacharyya et al. (2022) proposed that LY CMa could be an evolved Be star located between main sequence stars and supergiants on the optical color–magnitude diagram. If this is so, MAXI J0709 should have an intermediate character between Be X-ray binaries (BeXBs) and supergiant X-ray binaries (sgXBs).

BeXBs usually cause outbursts lasting for several weeks (type-I) to a few months (type-II), according to the interaction between the neutron star magnetosphere and the Be disk (e.g., Reig 2011; Sugizaki et al. 2017). The behavior is quite different from the present MAXI J0709 results.

However, a few BeXBs, such as X Persei, are known to show short-time-scale variabilities like flares (Delgado-Martí et al. 2001; Acuner et al. 2014). MAXI J0709 could be considered as an extreme case.

Recently, another new subclass of HMXBs, involving supergiant B[e] (sgB[e]) stars as mass-donating companions, has been getting a great deal of attention (e.g., Kraus 2019). The sgB[e] stars are thought to accompany dense, dusty disks. The two members of this subclass, CI Cam (Bartlett et al. 2019) and IGR J16318−4848 (Fortin et al. 2020), are known to exhibit extremely high ($\gtrsim 10^{24}$ cm^{-2}) and variable $N_{\rm H}$ on their persistent X-ray activities. Although LY CMa is not definitely categorized into sgB[e], the thick and variable X-ray absorption feature in these two objects is quite similar with that observed in MAXI J0709 (subsection 2.2). This naturally leads to the idea that some sgB[e] HMXBs may behave like SFXTs. A candidate for such objects, namely sgB[e]FXTs, has already been reported (Sidoli et al. 2022). Further observations of LY CMa would give us useful hints about possible relationships between these HMXB subclasses.

8 Conclusion

On 2022 January 25, MAXI discovered the new bright X-ray transient MAXI J0709−159 lasting for ∼3 hr in the constellation Canis Majoris. Prompt follow-up observations with NICER and NuSTAR confirmed the new X-ray object and refined the source position with 20″ accuracy. Then, the optical counterpart was identified with LY CMa, which has been identified as B supergiant and also a Be star. Detailed analysis of MAXI and NuSTAR data has revealed a characteristic X-ray outburst represented by a short duration (∼3 hr), rapid ($\lesssim$ a few seconds) variability accompanied by spectral change, and a large luminosity swing from quiescence ($\sim 10^{32}$ erg s^{-1}) to the flare peak ($\sim 10^{37}$ erg s^{-1}). These features agree well with typical SFXTs. The spectral change during the short outburst period suggests that the $N_{\rm H}$ increased from 10^{22} to 10^{23} cm^{-2}, which can be explained by a scenario in which the compact object (a neutron star) just plunged into a dense clump in the circumstellar medium. Meanwhile, the optical spectroscopic observation of LY CMa reveals a broad Hα emission line, suggesting the existence of a circumstellar Be disk. However, the observed X-ray behavior agrees with SFXTs, i.e., supergiant X-ray binaries, rather than Be X-ray binaries. Thus, LY CMa is surrounded by a complex circumstellar medium including dense clumps. These facts suggest that the object could be classified into an intermediate position between these HMXB subclasses, namely an evolved Be fast X-ray transient.

Acknowledgement

The authors thank the MAXI team members for their dedicated work on the mission operation. M. Sugizaki acknowledges support from the Chinese Academy of Sciences (CAS) President's International Fellowship Initiative (PIFI) (grant No. 2020FSM004). Part of this work was financially supported by Grants-in-Aid for Scientific Research 17H06362 (TM, HN, NK), 19K14762 (M. Shidatsu), and 21K03620 (HN) from the Ministry of Education, Culture, Sports, Science and Technology (MEXT) of Japan. We thank the NuSTAR and Swift operation teams for performing the ToO observations, and Brian Grefenstette for the quick-look analysis of the NuSTAR data. This work is based on data from eROSITA, the soft X-ray instrument aboard SRG, a joint Russian–German science mission supported by the Russian Space Agency (Roskosmos), in the interests of the Russian Academy of Sciences represented by its Space Research Institute (IKI) and the Deutsches Zentrum für Luft- und Raumfahrt (DLR). The SRG spacecraft was built by the Lavochkin Association (NPOL) and its subcontractors, and is operated by NPOL with support from the Max Planck Institute for Extraterrestrial Physics (MPE). The development and construction of the eROSITA X-ray instrument was led by MPE, with contributions from the Dr Karl Remeis Observatory Bamberg and ECAP (FAU Erlangen-Nuernberg), the University of Hamburg Observatory, the Leibniz Institute for Astrophysics Potsdam (AIP), and the Institute for Astronomy and Astrophysics of the University of Tübingen, with the support of DLR and the Max Planck Society. The Argelander Institute for Astronomy of the University of Bonn and the Ludwig Maximilians Universität Munich also participated in the science preparation for eROSITA. This work has also made use of data from the European Space Agency (ESA) mission Gaia (https://www.cosmos.esa.int/gaia), processed by the Gaia Data Processing and Analysis Consortium (DPAC, https://www.cosmos.esa.int/web/gaia/dpac/consortium). Funding for the DPAC has been provided by national institutions, in particular the institutions participating in the Gaia Multilateral Agreement. The Digitized Sky Surveys were produced at the Space Telescope Science Institute under US Government grant NAG W-2166. The images of these surveys are based on photographic data obtained using the Oschin Schmidt Telescope on Palomar Mountain and the UK Schmidt Telescope. The plates were processed into the present compressed digital form with the permission of these institutions. The National Geographic Society Palomar Observatory Sky Atlas (POSS-I) was made by the California Institute of Technology with grants from the National Geographic Society. The Second Palomar Observatory Sky Survey (POSS-II) was made by the California Institute of Technology with funds from the National Science Foundation, the National Geographic Society, the Sloan Foundation, the Samuel Oschin Foundation, and the Eastman Kodak Corporation. The Oschin Schmidt Telescope is operated by the California Institute of Technology and Palomar Observatory. The UK Schmidt Telescope was operated by the Royal Observatory Edinburgh, with funding from the UK Science and Engineering Research Council (later the UK Particle Physics and Astronomy Research Council) until 1988 June, and thereafter by the Anglo-Australian Observatory. The blue plates of the Southern Sky Atlas and its equatorial extension (together known as SERC-J), as well as the Equatorial Red (ER), and the Second Epoch [red] Survey (SES) were all taken with the UK Schmidt. Supplemental funding for sky-survey work at the ST ScI is provided by the European Southern Observatory.

References

Acuner, Z., İnam, S. Ç., Şahiner, Ş., Serim, M. M., Baykal, A., & Swank, J. 2014, MNRAS, 444, 457

Arnaud, K. A. 1996, ASP Conf. Ser., 101, 17

Bachetti, M., & Huppenkothen, D. 2018, ApJ, 853, L21

Bailer-Jones, C. A. L., Rybizki, J., Fouesneau, M., Demleitner, M., & Andrae, R. 2021, AJ, 161, 147

Bartlett, E. S., Clark, J. S., & Negueruela, I. 2019, A&A, 622, A93

Bhattacharyya, S., et al. 2022, ApJ, 933, L34

Boller, T., Freyberg, M. J., Trümper, J., Haberl, F., Voges, W., & Nandra, K. 2016, A&A, 588, A103

Bozzo, E., et al. 2011, A&A, 531, A130

Bozzo, E., Falanga, M., & Stella, L. 2008, ApJ, 683, 1031

Bozzo, E., Romano, P., Ducci, L., Bernardini, F., & Falanga, M. 2015, Adb. Space Res., 55, 1255

Bozzo, E., Stella, L., Ferrigno, C., Giunta, A., Falanga, M., Campana, S., Israel, G., & Leyder, J. C. 2010, A&A, 519, A6

Brunner, H., et al. 2022, A&A, 661, A1

Cash, W. 1979, ApJ, 228, 939

Chojnowski, S. D., et al. 2015, AJ, 149, 7

Delgado-Martí, H., Levine, A. M., Pfahl, E., & Rappaport, S. A. 2001, ApJ, 546, 455

Ferrigno, C., Bozzo, E., & Romano, P. 2020, A&A, 642, A73

Fortin, F., Chaty, S., & Sander, A. 2020, ApJ, 894, 86

Gaia Collaboration 2016, A&A, 595, A1

Gaia Collaboration 2021, A&A, 649, A1

Gehrels, N., et al. 2004, ApJ, 611, 1005

Gendreau, K. C., Arzoumanian, Z., & Okajima, T. 2012, SPIE Proc., 8443, 844313

Giménez-García, A., Torrejón, J. M., Eikmann, W., Martínez-Núñez, S., Oskinova, L. M., Rodes-Roca, J. J., & Bernabéu, G. 2015, A&A, 576, A108

Grebenev, S. A., & Sunyaev, R. A. 2007, Astron. Lett., 33, 149

Harrison, F. A., et al. 2013, ApJ, 770, 103

HI4PI Collaboration 2016, A&A, 594, A116

Hori, T., et al. 2018, ApJS, 235, 7

Houk, N., & Smith-Moore, M. 1988, Michigan Catalogue of Two-Dimensional Spectral Types for the HD Stars, Vol. 4 (Ann Arbor: Department of Astronomy, University of Michigan)

Huppenkothen, D., et al. 2019, ApJ, 881, 39

Iwakiri, W., et al. 2022, Astron. Telegram, 15181, 1

Joye, W. A., & Mandel, E. 2003, ASP Conf. Ser., 295, 489

Kawai, H., Tsuboi, Y., Iwakiri, W. B., Maeda, Y., Katsuda, S., Sasaki, R., Kohara, J., & MAXI TEAM 2022, PASJ, 74, 477

Kobayashi, K., et al. 2022, Astron. Telegram, 15188, 1

Kraus, M. 2019, Galaxies, 7, 83

Kretschmar, P., et al. 2019, New Astron. Rev., 86, 101546

Lansbury, G. B., et al. 2017, ApJ, 836, 99

Leahy, D. A., Darbro, W., Elsner, R. F., Weisskopf, M. C., Sutherland, P. G., Kahn, S., & Grindlay, J. E. 1983, ApJ, 266, 160

Matsuoka, M., et al. 2009, PASJ, 61, 999

Mihara, T., et al. 2011, PASJ, 63, S623

Mihara, T., Tsunemi, H., & Negoro, H. 2022, MAXI: Monitor of All-sky X-ray Image, in Handbook of X-ray and Gamma-ray Astrophysics, ed. C. Bambi & A. Santangelo (arXiv:2206.01505)

Morii, M., et al. 2013, ApJ, 779, 118

Morii, M., Yamaoka, H., Mihara, T., Matsuoka, M., & Kawai, N. 2016, PASJ, 68, S11

Negoro, H., et al. 2016, PASJ, 68, S1

Negoro, H., Mihara, T., Pike, S., Grefenstette, B., Iwakiri, W., Nakajima, M., & Gendreau, K. 2022, Astron. Telegram, 15193, 1

Nesci, R. 2022, Astron. Telegram, 15194, 1

Pavlinsky, M., et al. 2021, A&A, 650, A42

Pike, S. N., et al. 2022, ApJ, 927, 190

Pradhan, P., Bozzo, E., & Paul, B. 2018, A&A, 610, A50

Predehl, P., et al. 2021, A&A, 647, A1

Reig, P. 2011, Ap&SS, 332, 1

Rhodes, L., van den Eijnden, J., Fender, R., Woudt, P., & Miller-Jones, J. 2022, Astron. Telegram, 15209, 1

Serino, M., et al. 2022, Astron. Telegram, 15178, 1

Sguera, V., et al. 2006, ApJ, 646, 452

Shakura, N., Postnov, K., Kochetkova, A., & Hjalmarsdotter, L. 2012, MNRAS, 420, 216

Sidoli, L., & Paizis, A. 2018, MNRAS, 481, 2779

Sidoli, L., Sguera, V., Esposito, P., Oskinova, L., & Polletta, M. 2022, MNRAS, 512, 2929

Sugizaki, M., et al. 2011, PASJ, 63, S635

Sugizaki, M., Mihara, T., Nakajima, M., & Makishima, K. 2017, PASJ, 69, 100

Sunyaev, R., et al. 2021, A&A, 656, A132

Tsygankov, S. S., et al. 2022, A&A, 661, A45

Wilms, J., Allen, A., & McCray, R. 2000, ApJ, 542, 914